Broad-band acceleration time histories synthesis by coupling low-frequency ambient seismic field and high-frequency stochastic modelling

Loïc Viens, Aurore Laurendeau, Luis Fabian Bonilla, Nikolaï Shapiro

Geophysical Journal International

Geophys. J. Int. (2014) **199,** 1784–1797
GJI Seismology

doi: 10.1093/gji/ggu362

Broad-band acceleration time histories synthesis by coupling low-frequency ambient seismic field and high-frequency stochastic modelling

L. Viens,[1,2] A. Laurendeau,[3,*] L. F. Bonilla[4] and N. M. Shapiro[2]

[1]*Earthquake Research Institute, University of Tokyo,* 1-1-1 *Yayoi, Bunkyo-ku, Tokyo* 113-0032, *Japan. E-mail: viens@eri.u-tokyo.ac.jp*
[2]*Institut de Physique du Globe de Paris, Equipe de Sismologie, Paris, France*
[3]*Université Grenoble Alpes, ISTerre, F-*38041 *Grenoble, France*
[4]*Université Paris-Est, IFSTTAR, France*

Accepted 2014 September 12. Received 2014 September 2; in original form 2014 April 9

SUMMARY

In this study, information carried by the ambient seismic field is exploited to extract impulse response functions between two seismic stations using one as a 'virtual' source. Interferometry by deconvolution method is used and validated by comparing the extracted ambient noise impulse response waveforms with records of moderate magnitude earthquakes (from M_w 4 to 5.8) that occurred close to the virtual source station in Japan. As the information is only available at low frequencies (less than 0.25 Hz), the ambient seismic field approach is coupled to a non-stationary stochastic model to simulate time domain accelerograms up to 50 Hz. This coupling allows the predicted ground motion to have both the deterministic part at low frequencies coming from the source and the crust structure and the high-frequency random contribution from the seismic waves scattering. The resulting combined accelerograms for an M_w 5.8 event show a good agreement with observed ground motions from a real earthquake.

Key words: Interferometry; Earthquake ground motions; Asia.

1 INTRODUCTION

Earthquakes represent one of the most significant destructing natural hazards and could occur worldwide affecting a large population. In this context, ground motion predictions are critical to evaluate the seismic hazard in highly populated areas which, in some cases, include potentially hazardous activities such as nuclear power plants, chemical industry, dams, among other critical facilities.

One way to evaluate the seismic hazard is to simulate ground shaking, which might be provoked by future earthquakes. Many methods have been developed to provide broad-band realistic traces reproducing the time and frequency non-stationarity and the variability of the phenomena to engineers. Engineering methods, such as the one developed by Gasparini & Vanmarcke (1976), can be used to obtain artificial acceleration time-series. The purpose of this approach is to generate acceleration time histories whose response spectra match a target response spectrum. However, this method generates accelerograms, which are often unusable because of their unreasonably high-energy content (Bommer & Acevedo 2004). It also suffers from a lack of the earthquake physics and from the fact that the computed accelerograms are stationary and do not reproduce the earthquake variability (Pousse *et al.* 2006). A method more commonly used to provide temporal traces of the ground motion to engineers is the stochastic simulation method developed by Boore (1983) and subsequently improved (Boore 2003). This method has the advantage to be a physics-based method but needs to characterize numerous input parameters and does not simulate the non-stationarity and the variability of the signal. Thus, empirical models combining seismological information with engineering notions characterizing the non-stationarity in time and frequency have been developed such as the one of Pousse *et al.* (2006) improved by Laurendeau (2013). This method can simulate accelerograms with realistic energy, duration and frequency content by also reproducing the variability of the earthquakes. However, all these stochastic methods only represent the high-frequency wave scattering because the assumption of a random phase is acceptable only for frequencies higher than 1 Hz.

More physical methods, based on the fact that ground motions are a convolution of the source, path and site effects (Aki & Richards 2002) have also been developed such as the empirical Green's function method (e.g. Hartzell 1978; Irikura 1983). Unfortunately, this method presents two major drawbacks: (i) it only allows modelling for frequencies higher than the corner frequency of the small event and (ii) good-quality earthquake records have to be available in the studied area.

Following the increase of computational power Komatitsch *et al.* (2004) and Olsen *et al.* (2006) predict ground motion using

*Now at: CEA, DAM, DIF, F-91297 Arpajon, France.

simulations that include the rupture of the fault and the propagation of the radiated waves. However, a good knowledge of the media is required and the complexity of the source combined with the path and the site effects makes difficult accurate predictions at all frequencies.

In this paper, we explore a recently developed empirical approach that uses the correlation of the ambient seismic field (e.g. Campillo *et al.* 2011) to predict the ground motions at low frequencies. The correlation of seismic ambient field between two stations contains a coherent part, which is directly related to the Green's function, or impulse response, from one station with respect to the other. This approach has been introduced in seismology by Weaver & Lobkis (2001) and Lobkis & Weaver (2001). Then, Wapenaar (2004), Snieder (2004), Roux *et al.* (2005b) and Gouédard *et al.* (2008) proved that Green's functions in a 3-D media can be recovered and Campillo & Paul (2003) demonstrated the possibility to retrieve the Earth impulse responses in geophysics using late seismic coda. Shapiro & Campillo (2004) also used seismic field cross-correlations to extract the Rayleigh-wave part of the Green's function and Shapiro *et al.* (2005) used the dispersion of these waves to image the velocity structure under California. However, these methods using cross-correlations usually sacrifice the amplitude information to improve the resolution of the waves arrival time by applying one-bit normalization (Shapiro & Campillo 2004) or pre-whitening (Bensen *et al.* 2007) to the data.

To estimate seismic ground motions, the primary requirement is to keep both phase and amplitude of the impulse responses. To do so, Prieto & Beroza (2008) used deconvolution of the ambient seismic field without any pre-processing instead of cross-correlations to keep this information. They validated this method, which is also efficient to predict basin amplification effects in low-seismicity areas, by predicting accurately the ground motions of moderate magnitude earthquakes that occurred in the vicinity of the stations considered as the virtual sources. More recently, Denolle *et al.* (2013) corrected the surface impulse responses for source depth and for double-couple focal mechanism of the target earthquakes and Denolle *et al.* (2014) extended this method to a finite rupture to simulate ground motions of large-magnitude earthquakes. However, impulse responses are recoverable only at low frequency (up to 0.25 Hz). Thus, this method is only efficient to analyse the earthquake hazard of large engineering structures as tall buildings or bridges having long-period resonance.

To simulate realistic broad-band ground motions, hybrid schemes combining deterministic and stochastic methods have been developed by several authors (e.g. Kamae *et al.* 1998; Pulido & Kubo 2004; Causse *et al.* 2009). In these papers, the low-frequency content is evaluated by numerical simulations whereas the high-frequency content is simulated by stochastic modelling (Boore 1983) or by using the empirical Green's function method (Hartzell 1978). These methods successfully explain the general characteristics of ground motion of the Hyogo-ken Nanbu earthquake (Kamae *et al.* 1998) and the Tottori earthquake (Pulido & Kubo 2004). The method developed by Causse *et al.* (2009) predicts the ground motions in case of an M_w 5.5 event in the Grenoble basin in the French Alps. However, the methods used to simulate the low-frequency content require a good knowledge of the velocity model and the high-frequency simulations present the drawbacks previously described.

In this study, the low-frequency ambient seismic field analysis is coupled to the non-stationary stochastic simulation method developed by Pousse *et al.* (2006) and improved by Laurendeau (2013). Extraction of impulse responses from the ambient seismic field do not required any knowledge of the velocity structure and the method of Laurendeau (2013), which is calibrated for Japan using the data recorded at the surface by the KiK-net and K-NET networks, allows to reproduce the non-stationarity in time and frequency of the signal at high frequencies. We use the complementary power of both methods to predict realistic ground motions in the northern Tokyo area (Fukushima, Ibaraki, Tochigi, Yamagata and Niigata prefectures) generated by an M_w 5.8 earthquake. The choice of this area is based on the fact that many shallow earthquakes of various magnitudes happened in the northern part of Ibaraki prefecture close to one Hi-net station and are used to validate the method.

In this paper, we first describe the networks and data that we used. Then, we present the methods to compute the ambient noise impulse responses, the non-stationary stochastic simulations and the combination of both to provide a hybrid scheme. Finally, results of each method are shown followed by a discussion.

2 SEISMIC NETWORKS

After the Hyogo-Ken Nanbu earthquake, which struck the Kobe area in 1995, a national project started to improve the seismic observation systems in Japan. This project aimed to build dense and uniform networks covering the whole country to understand better earthquake phenomena and to mitigate related disasters. Different types of networks have been deployed to record broad-band and strong motion data. In this study, we first describe the Hi-net network recording continuous data that we used to perform ground motion predictions in Japan at low frequencies. Then, we describe the K-NET and KiK-net networks used to construct the models to perform the high-frequency stochastic simulations.

2.1 Hi-net network and data set

The Hi-net network is operated by the National Research Institute for Earth Sciences and Disaster Prevention (NIED) and is composed of approximately 800 stations covering uniformly the whole Japan. To avoid surface ground noise and record stable high-quality data, sensors are installed at the bottom of boreholes of at least 100 m up to 3500 m depth (Okada *et al.* 2004; Obara *et al.* 2005).

The Hi-net stations considered in this study are represented in Fig. 1 by triangles. The colour of these triangles represents the average shear wave velocity in the first 30 m depth, also called V_{S30}. Station names framed by a rectangle are the ones for which we present the combined accelerograms in Section 4.3. To validate the ambient seismic field deconvolution method, a comparison between computed ambient noise impulse responses and earthquake records is necessary. Events located in the surrounding of JUOH and THGH stations have been selected (Table 1) and two of them of magnitude M_w 5.02 and 5.82 are shown in Fig. 1. Mechanisms of the selected earthquakes correspond to normal faulting.

Every Hi-net station is equipped with a three-component high-sensitivity velocity seismometer recording continuous seismic waveforms. Seismometers have a natural frequency of 1 Hz and a sensitivity of 200 V m^{-1} s^{-1}. 24 bits analog-to-digital (A/D) converters with a sampling frequency of 2 kHz are used to digitize the data, which are finally decimated to a sampling frequency of 100 Hz. As explained by Obara *et al.* (2005), Hi-net sensors are short-period seismometers with a flat response above 1 Hz. As the information carried by the ambient seismic field is only at low frequency, velocity records are deconvolved by their instrument response functions to recover the real amplitude of long-period seismic waves (below 1 Hz). Fig. 2 shows the velocity power spectral density (PSD) of raw data (grey line) and data corrected of their instrument response

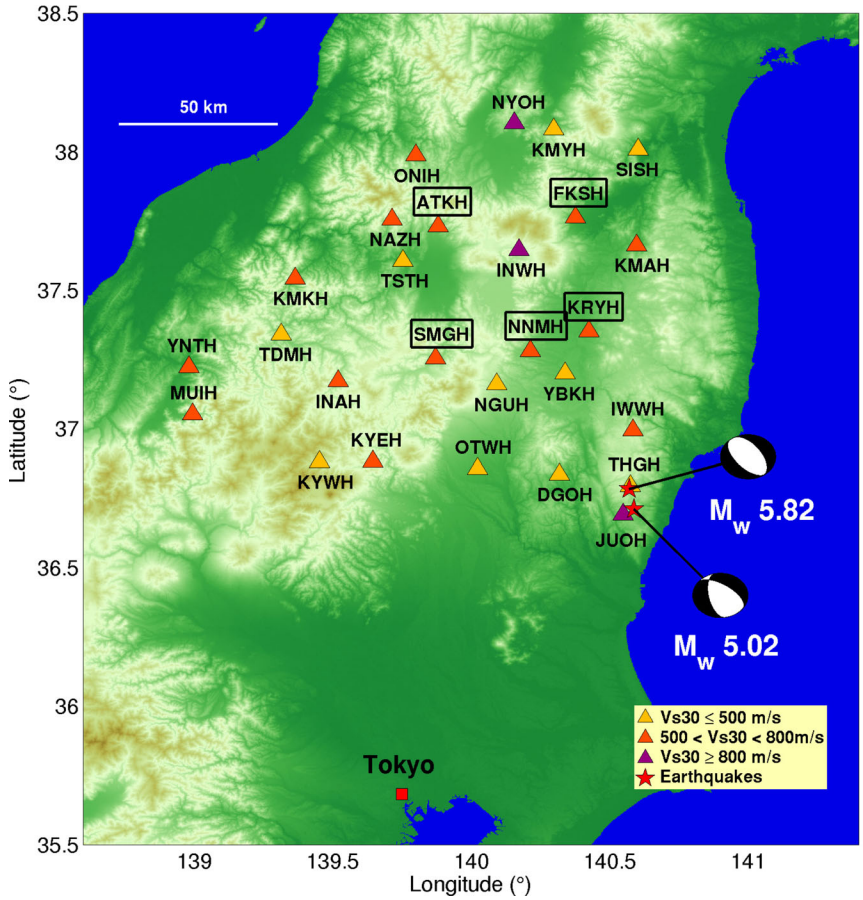

Figure 1. Northern Tokyo area map, including selected Hi-net stations (triangles) and the location of the M_w 5.02 and 5.82 earthquakes (stars). The colour of the triangles represents the average shear wave velocity in the first 30 m depth (V_{S30}). Station names framed by a rectangle are the ones for which we present the combined accelerograms in Section 4.3. The colour version of this figure is available only in the electronic edition.

Table 1. Characteristics of the considered earthquakes.

Origin time (JST[a])	M_w [b]	Latitude	Longitude	Depth (km)	Distance epicentre: JUOH station (km)	Strike / Dip / Rake
2011/06/02 14:47:52.54	4.01	36.825N	140.586E	5	15.1	12 / 43 / −111
2011/04/02 19:22:54.54	4.15	36.820N	140.569E	5	14.3	344 / 23 / −104
2011/04/05 18:08:49.24	4.33	36.808N	140.566E	5	13.0	311 / 24 / −134
2011/08/16 19:16:13.74	4.44	36.827N	140.573E	5	15.1	334 / 23 / −125
2011/05/26 19:56:36.24	4.61	36.719N	140.624E	5	7.3	343 / 34 / −75
2011/04/14 07:35:49.78	4.89	36.778N	140.573E	5	9.8	314 / 29 / −109
2011/11/20 10:23:40.78	5.02	36.711N	140.588E	5	4.1	307 / 47 / −122
2011/09/21 22:30:57.12	5.15	36.737N	140.577E	5	5.6	340 / 32 / −93
2011/03/19 18:56:48.06	5.82	36.784N	140.571E	5	10.4	328 / 44 / −85

[a]Japan Standard Time (UT + 9:00).
[b]Moment magnitude.

(black line). 1 hr signal recorded in 2010 August at DGOH station by the vertical component has been used. Up to 1 Hz, the amplitude of the instrument response corrected PSD is significantly higher than the amplitude of the raw signal PSD. Moreover, the instrument response removal allows to recover data with energy level higher than the new low noise model (NLNM) of Peterson (1993). Above 1 Hz, both PSDs have the same shape.

2.2 K-NET and KiK-net networks

K-NET network is made of approximately 1000 stations covering the whole Japan with a spacing of 25 km at the surface (Okada *et al.* 2004). Conversely, KiK-net network is composed of 669 stations. Hi-net and KiK-net networks have co-located seismometers and accelerometers in the boreholes, respectively. Instrumentation used for K-NET and KiK-net is basically the same. Each station is composed of a three-component accelerometer and an A/D converter with a resolution of 24 bits. The sampling rate is 100 Hz for K-NET and 200 Hz for KiK-net (Aoi *et al.* 2004).

To validate the instrument response correction of the Hi-net data, corrected and raw Hi-net records of an M_w 5.82 earthquake (*cf.* Table 1) at DGOH station (see Fig. 1 for location) are compared to KiK-net records. Data are first bandpass filtered between 0.05 and 2 Hz and decimated up to a Nyquist frequency of 2 Hz. Finally, raw

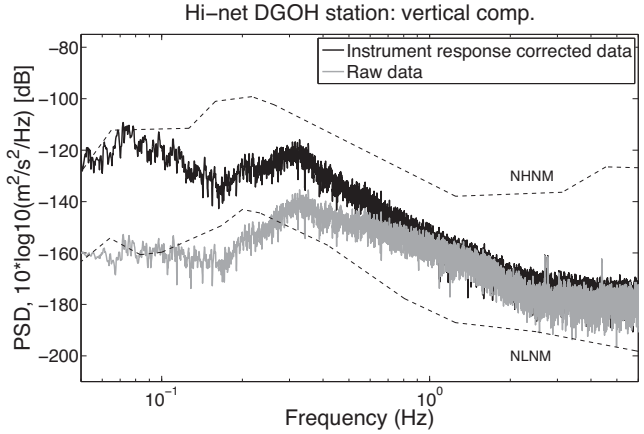

Figure 2. Velocity power spectral density (PSD) of raw Hi-net data (grey line) and instrument response corrected data (black line). 1 hr signal recorded in 2010 August at DGOH station by the vertical component has been used. We also show the new low noise model (NLNM) and the new high noise model (NHNM) by Peterson (1993) (dashed lines).

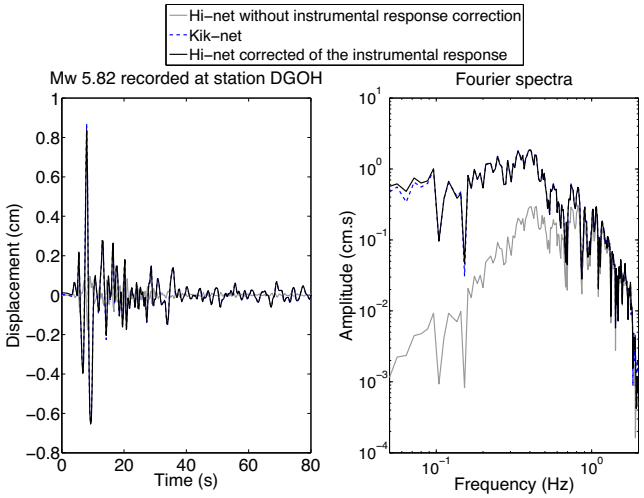

Figure 3. KiK-net (dashed line), Hi-net raw data (grey line) and instrument response corrected Hi-net data (black line) displacement time histories (left-hand side) and Fourier displacement spectra (right-hand side) of the vertical component for an M_w 5.82 earthquake recorded by the DGOH station. The colour version of this figure is available only in the electronic edition.

and instrument response corrected Hi-net records are integrated once and borehole KiK-net data are integrated twice to retrieve the corresponding displacement. Results are shown for the vertical component in Fig. 3. A good match in time and frequency domain can be observed between corrected Hi-net and KiK-net records in the frequency range of 0.05 to 2 Hz even if a small difference between both spectra can be observed below 0.1 Hz. The amplitude of the raw Hi-net data is however significantly lower below 1 Hz. In the following, we use the corrected Hi-net data to compute the ambient noise impulse responses and the KiK-net data to compare the results of our combined simulations with earthquake records.

3 METHODS

3.1 Computation of the ambient noise impulse response functions

Prior to go through the computation of ambient noise impulse response functions using the deconvolution technique, some data preprocessing is required. First, Hi-net raw data are converted from WIN32 format [based on the 'WIN system' developed by Earthquake Research Institute (ERI), The University of Tokyo] to SAC (Seismic Analysis Code) format, divided into 1-hr time windows, and corrected for their instrument responses. Then, as the ambient seismic field is only coherent at low frequencies and to speed up the computation of the impulse response functions, a bandpass filter is applied to the seismograms between 0.05 and 2 Hz followed by a decimation from 100 Hz down to 4 Hz to keep the information up to a Nyquist frequency of 2 Hz. Data are then rotated from the coordinate system north-east-down to radial-transverse-down by considering JUOH station as the virtual source. Finally, to exclude possible earthquake records of the data set used to compute the ambient noise impulse responses, time-series with spikes larger than 10 times the standard deviation of the window are excluded as done by Denolle *et al.* (2013).

After this pre-processing, ambient noise impulse responses are computed using deconvolution in the frequency domain between records at two stations with one station considered as the virtual source (point force) and the other one as the receiver. To obtain signal spectra with little or no bias and small uncertainties to minimize the spectral leakage, we used the multitaper spectrum analysis introduced by Thomson (1982) and more specifically the library developed by Prieto *et al.* (2009). The deconvolution is defined in the frequency domain for each pair of stations and each component as

$$\widehat{ANIR}_{ij}(x_r, x_s, \omega) = \left\langle \frac{\hat{u}_i(x_r, \omega)\hat{u}_j^*(x_s, \omega)}{\{|\hat{u}_j(x_s, \omega)|\}^2 + \xi} \right\rangle, \quad (1)$$

with $\widehat{ANIR}(x_r, x_s, \omega)$ being the ambient noise impulse response. x_s and x_r are, respectively, the virtual source and receiver positions and ω is the frequency. i and j are respectively the i-th component of velocity at the receiver position and the j-th component of velocity at the source position. Asterisk $*$ denotes the complex conjugate, operator $\langle\rangle$ means the stack of 1 hr time-series over 1 month and $\{\}$ denotes a smoothing of the virtual source spectra computed by using a moving average over 20 points to keep stability in the deconvolution because the spectrum in the denominator $\hat{u}_j$ can almost reach zero near the notches involving an unstable deconvolution. Moreover, a water level ξ is also used to keep stable the deconvolution. This water level is set to 1 per cent of the average spectral power (e.g. Prieto & Beroza 2008; Denolle *et al.* 2013).

Because each station is equipped with a three-component seismometer, a nine-component rank two tensor of ambient noise impulse responses is extracted for each pair of stations. The inverse Fourier transform of the causal part of the ambient noise impulse responses is then applied to obtain waveforms in time domain. Even if the deconvolution process should remove the effect of the noise source as demonstrated by Vasconcelos & Snieder (2008), a strong variability over 1 yr is observed in the studied area. Between 2010 August and 2011 August, impulse responses computed using data recorded in 2010 August have the highest signal-to-noise ratio and thus, are the ones used in the following.

The deconvolution method only extracts relative, rather than absolute, amplitude of the impulse responses. Prieto & Beroza (2008)

and Denolle *et al.* (2013) defined the ambient noise impulse response tensor to be proportional to the Green's tensor of the surface waves up to a normalization factor for each component (λ_{ij}), but common to all the station pairs, as

$$G_{ij}(x_r, x_s, t) = \lambda_{ij} \times ANIR_{ij}(x_r, x_s, t). \quad (2)$$

The computation of these normalization factors uses records of an earthquake located in the close vicinity of the station considered as the virtual source. In this study, only the diagonal terms of the impulse response tensor are compared to the earthquake records. Normalization factors λ_{RR}, λ_{TT} and λ_{ZZ} are computed as:

(i) FFT of impulse responses ($\widehat{ANIR}$) and earthquake records ($\widehat{E}$) are computed for all the considered stations (N_s).

(ii) Absolute values of the Fourier spectra between the two cut-off frequencies ($f_{\min}$ and $f_{\max}$) of the bandpass filter are summed.

(iii) Values obtained at the previous step are summed over the number of considered stations for both the earthquake and the noise impulse response data.

(iv) Ratio between the two values obtained at the previous step is calculated to obtain λ_{ii}.

Mathematically, this factor can be expressed as

$$\lambda_{ii} = \frac{\sum_{n=1}^{N_s} \sum_{f=f_{\min}}^{f_{\max}} |\widehat{E}_{ii}(n, f)|}{\sum_{n=1}^{N_s} \sum_{f=f_{\min}}^{f_{\max}} |\widehat{ANIR}_{ii}(n, f)|}. \quad (3)$$

To compare the phases of earthquake and impulse response waveforms at each station, Denolle *et al.* (2013) suggested to calculate normalized correlation coefficients *CC* in time domain as

$$CC = \frac{\sum_{i=N_{2.5}}^{N_{92.5}} u_i v_i}{\sqrt{\sum_{i=N_{2.5}}^{N_{92.5}} u_i^2 v_i^2}}, \quad (4)$$

with u being the impulse response function and v being the earthquake record in time domain. $N_{2.5}$ and $N_{92.5}$ correspond, respectively, to 2.5 and 92.5 per cent of the cumulative energy of both signals (sum of the time-series values squared).

As earthquakes and the virtual source station are not exactly colocated, a phase time delay between earthquake records in velocity and impulse responses is observed. To correct this time-shift, we first calculated the distance difference between the virtual source and the receiver and between the earthquake hypocentre and the receiver. This distance is then divided by a theoretical velocity of the surface waves (e.g. 3.2 km s^{-1}) and the earthquake occurring time is corrected from this value.

Finally, several sources of uncertainties need to be taken into account. First, impulse responses are not corrected for the excitation depth using a velocity model and the focal mechanism of the event as it has been done recently by Denolle *et al.* (2013). Moreover, uncertainties on the earthquake location and its occurring time can also induce some mismatches between earthquake and impulse response wave arrival times. To take these uncertainties into account, we allow a free phase shift of 1.5 s and keep the occurring time which maximize the correlation coefficient between both waveforms.

3.2 High-frequency non-stationary stochastic simulations

To obtain ground motions usable at higher frequencies, the ambient seismic field technique is used together with a non-stationary stochastic method to simulate the time histories of horizontal components up to 50 Hz. Here, the non-stationary (in time and frequency) semi-empirical stochastic method developed by Sabetta & Pugliese (1996), modified by Pousse *et al.* (2006) with improvements of Laurendeau (2013) is used. Among the available techniques for generating time histories at high frequencies, this method has the advantage of being simple (it does not require detailed knowledge on the rupture, travel path or site conditions) and accounting for basic concepts of seismology (Brune's source, a realistic envelope function, non-stationarity and variability); see Douglas & Aochi (2008) for a review of the advantage and the disadvantage of this type of techniques. Time-domain simulations are derived from the signal spectrogram and depend on the distributions of three intensity parameters. First the Arias intensity (*AI*), which is a measure of the signal energy (Arias 1970). Second, the relative significant duration (D_{SR}), which is the time interval between 5 and 95 per cent of the cumulative *AI* over time (Husid 1969). Finally, the evolution of the central frequency over the time ($F_C(t)$), parameter describing the non-stationarity, is related to the spectral moments of the power spectrum density (Lai 1982). The distributions are given by ground motion prediction equations (GMPEs). In the study of Laurendeau (2013), these indicators are characterized from KiK-net and K-NET accelerometric data recorded on surface rock and stiff-soil sites ($V_{S30} > 500$ m s^{-1}).

The basis of the non-stationary stochastic method of Sabetta & Pugliese (1996), Pousse *et al.* (2006) and Laurendeau (2013) are the stationary stochastic method of Gasparini & Vanmarcke (1976). This method assumes that a periodic function can be decomposed into a series of sines or cosines as

$$x(t) = \sum_{n=1}^{N} C_n(t) \cos(n2\pi \mathrm{d}f t + \varphi_n), \quad (5)$$

$$\text{with} \quad C_n(t) = \sqrt{2PS(t, f_n)\mathrm{d}f}, \quad (6)$$

in which $x(t)$ is the synthetic accelerogram in cm s^{-2}, the phases φ_n are random numbers uniformly distributed in the range $-\pi$ to π , and $PS(t, f)$ is the PSD (spectrogram). This assumption of random phase is acceptable above 1 Hz due to heterogeneities of the wave propagation medium. Sabetta & Pugliese (1996) assume that $PS(t,f)$ can be decomposed as

$$PS(t, f) = PS_\tau(f).Pa(t), \quad (7)$$

in which $PS_\tau(f)$ is the PSD at each sample time t and $Pa(t)$ is the envelop function. In their work, $PS_\tau(f)$ and $Pa(t)$ are represented by a log-normal density functions. The PSD at each sample time $PS_\tau(f)$ depends on the central frequency ($F_C(t)$), whereas $Pa(t)$ depends on Arias intensity (*AI*) and relative significant duration (D_{SR}) predictions. Pousse *et al.* (2006) and Laurendeau (2013) distinguish their works from the one of Sabetta & Pugliese (1996) by including basic concepts of seismology in the definition of all these functions. Indeed, $PS_\tau(f)$ is represented by a spectral density of a point source following the ω-square model (Frankel *et al.* 1996). The ω-square model is characterized by the corner frequency f_c and the maximum frequency f_{m_τ}, representing the high-frequency anelastic attenuation (e.g. Hanks 1982; Boore 2003). Since the central frequency decreases with time, $PS_\tau(f)$ becomes narrower at the end of the signal as shown in Fig. 4 (top panel). Furthermore, another improvement of this technique is the differentiation of the envelopes of *P*, *S* and Coda waves, respectively, also shown in Fig. 4 (middle

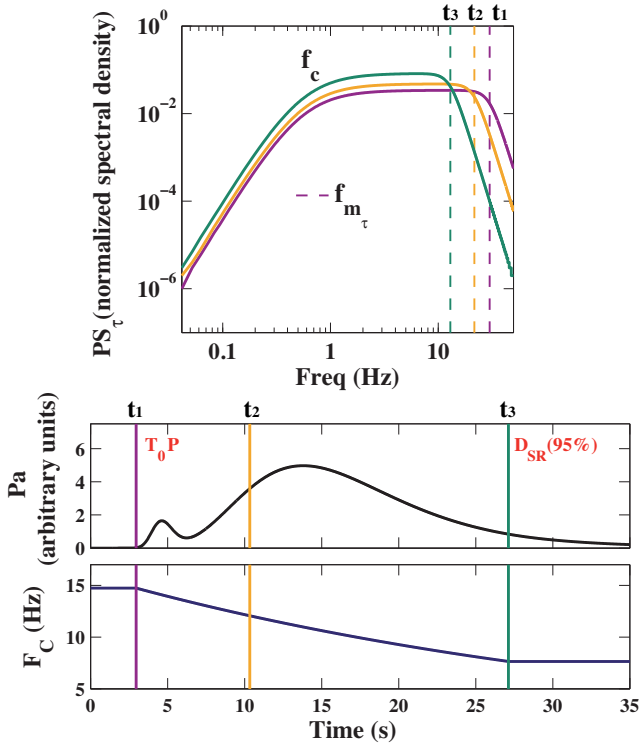

Figure 4. Illustration of function $PS_\tau(f)$ (eq. 6) describing the evolution of the spectral density (top panel), the time envelopes of the *P*, *S* and coda waves (middle panel), and the central frequency (bottom panel) as a function of time. To see the non-stationary behaviour of the spectral content, the spectral density (top panel) is shown at three different times (t_1–t_3) corresponding to the vertical lines in the lower figures. The colour version of this figure is available only in the electronic edition.

panel). Finally, the non-stationary behaviour is modelled by the central frequency (evolution of predominant frequency as a function of time) as indicated in the bottom panel of Fig. 4.

Recently, Laurendeau (2013) made three main improvements:

(i) A better characterization of the indicator distributions: The strong ground motion parameters are defined from a new database including the crustal accelerometric KiK-net and K-NET records on surface rock and stiff-soil sites until the end of 2009. New rock and stiff-soil prediction equations have been developed by taking into account the recent development of these models: analysis of both intra- and intervariability (Abrahamson & Youngs 1992), updated functional forms (e.g. Boore & Atkinson 2008; Foulser-Piggott & Stafford 2012; Bommer *et al.* 2009), incorporation of the scaling relations (e.g. Cotton *et al.* 2008) and V_{S30}.

(ii) A better characterization of the non-stationarity: To assess the variation of the frequency content over time, the Stockwell *et al.* (1996) transform of the signals has been used. With this technique, it is now possible to follow the evolution of the central frequency with a high resolution at each time step.

(iii) A better reproduction of the variability: In Pousse *et al.* (2006) method, each distribution was explored independently to reproduce the observed variability. The existing correlations between the input parameters have been analysed both for the inter- and the intracorrelations in order to better explore the joint distributions.

All these methods simulate the high-frequency behaviour of horizontal components only. The reader is welcome to read Pousse *et al.* (2006) and Laurendeau (2013) for details on the method.

3.3 Combination of the two methods

In this study, we only combined the two methods for stations located on surface rock and stiff-soil site ($V_{S30} > 500$ m s^{-1}) and we focused more particularly on NNMH, KRYH, SMGH, FKSH and ATKH stations by considering JUOH station as the virtual source. Once results from both methods have been obtained for these five stations, the combination is done as follows:

(i) First, ambient noise impulse responses are set to zero up to 1.5 s before the earthquake *P*-wave arrival time. From 1.5 s to the *P*-wave arrival time, data are multiplied by the first half of a Hanning window to taper the signal.

(ii) Second, ambient noise impulse responses are interpolated to the same sampling rate of the stochastic simulations ($\Delta t = 0.01$ s) and multiplied by the normalization factor to calibrate the amplitude.

(iii) Then, stochastic simulations are integrated once to retrieve the corresponding velocity and a high-pass filter with a cut-off frequency of 0.25 Hz (Butterworth filter, four poles and two passes) is applied. In addition, a low-pass filter with the same cut-off frequency is applied to the ambient noise impulse responses.

(iv) Finally, ambient noise impulse responses and stochastic simulations are summed in time domain as shown in Fig. 5.

4 RESULTS

4.1 Ambient noise impulse response results

4.1.1 On the nature of the ambient noise impulse responses

For each station, time-frequency analysis is performed for the *Z*–*Z* component of the ambient noise impulse response ($ANIR_{zz}(t,f)$) by using the Stockwell-transform (Stockwell *et al.* 1996) as

$$ANIR_{zz}(t,f) = \int_{-\infty}^{+\infty} ANIR_{zz}(\tau)\frac{|f|}{\sqrt{2\pi}}e^{-\frac{(t-\tau)^2 f^2}{2}}e^{-i2\pi f\tau}d\tau, \quad (8)$$

with $ANIR_{zz}(\tau)$ being the temporal ambient noise impulse response of the *Z*–*Z* component and *f* being the frequency.

Normalized Stockwell-transforms of five stations located between 11.7 and 139.4 km from the virtual source are shown in Fig. 6. This analysis shows that information can be recovered up to 1.4 Hz for short interstation distance (e.g. THGH station). Retrieval of information up to frequencies of engineering interest is consistent with the study of Roux *et al.* (2005a) who showed that information can be retrieved up to 1.3 Hz for stations located at less than 11 km from each other by using the cross-correlation method. Roux *et al.* (2005a) also demonstrated that body waves can be retrieved for short interstation distances. However, more investigations are needed to know if body waves can be also retrieved using interferometry by deconvolution. As the interstation distance increases, the recoverable frequency range decreases. At DGOH station, information can be recovered up to 0.9 Hz. For interstation distances larger than 50 km (e.g. KYEH, FKSH, and NAZH stations), high amplitudes are observed at lower frequencies (below 0.4 Hz). Moreover, a clear wave dispersion effect can be observed and indicates the recovery of surface waves. This feature is consistent with the work of Prieto & Beroza (2008) and Denolle *et al.* (2013) who made the assumption that only surface waves are retrieved for stations located at more than 100 km from the virtual source.

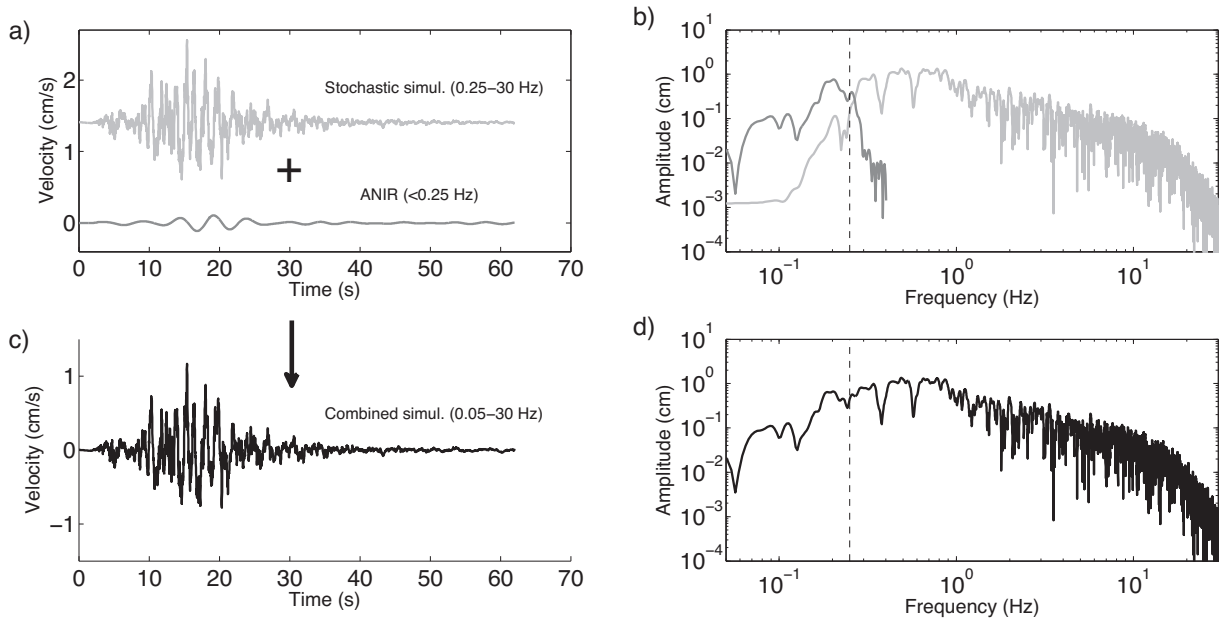

Figure 5. Principle of the coupling of the stochastic simulations and the ambient noise impulse responses in velocity. Low-pass filtered at 0.25 Hz ambient noise impulse response and one of the stochastic simulations integrated once to retrieve the corresponding velocity and high-pass filtered at 0.25 Hz are summed in time domain (a) to generate the combined simulation (c). Fourier spectra of the ambient noise impulse responses and the stochastic simulation are plotted in (b) and combined simulation Fourier spectrum is plotted in (d).

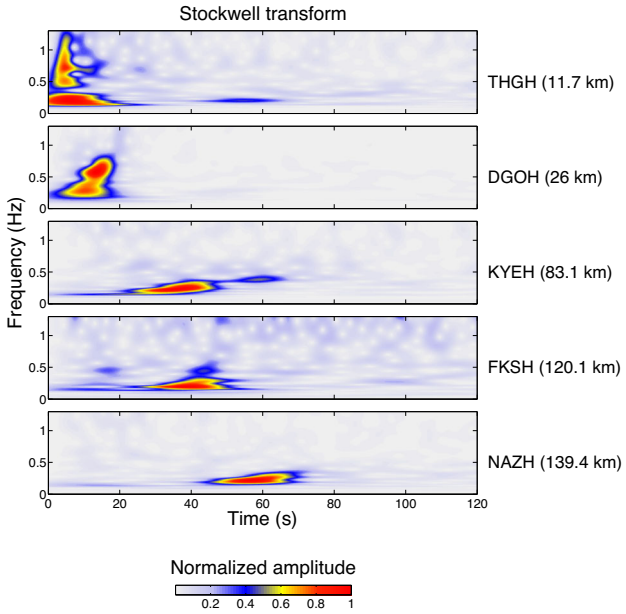

Figure 6. Time–frequency analyses of the *Z–Z* component ambient noise impulse responses computed with the Stockwell transform between the virtual source JUOH and stations located at 11.7 (THGH), 26 (DGOH), 83.1 (KYEH), 120.1 (FKSH) and 139.4 km (NAZH). For each station, the amplitude is normalized with respect to its maximum value. The colour version of this figure is available only in the electronic edition.

4.1.2 Comparison with earthquake records

As explained previously, ambient noise impulse response amplitudes need to be calibrated when compared to earthquake waveforms (eq. 2). Fig. 7 shows the *Z–Z* component of the impulse responses multiplied by the calibration factor λ_{ZZ} and vertical component of an M_w 4.61 earthquake records in velocity. Signals are bandpass filtered between 0.05 and 0.25 Hz and showed for stations located between 11.5 and 165 km from JUOH station. A good agreement of both waveforms can be observed for every station. Indeed, most of the stations have a correlation coefficient higher than 0.8 and similar amplitudes which validates the use of the ambient seismic field for ground motion prediction. A similar amplitude decrease of the ambient noise impulse response and the earthquake waves with the distance caused by geometrical spreading can be observed as well as local wave amplifications at NGUH and KYEH stations. Moreover, waves produced by the earthquake propagate faster northwards than westwards. This behaviour is also retrieved by the ambient noise impulse responses.

The waveform misfit that still remains can be explained by the fact that waves have a slightly different path as the earthquake and the virtual source are not exactly colocated. Moreover, the source mechanism of the earthquake may induce radiation effects that are not taken into account in the ambient noise impulse responses (Denolle *et al.* 2013). Yet, the resemblance of the reconstituted waveform using noise data is quite outstanding.

This earthquake and all the others (Table 1) are also located in the vicinity of THGH station. If this station is considered as the virtual source, similar results are observed when ambient noise impulse responses are compared to the earthquake records. In the following, even if earthquakes are located closer to THGH station than to JUOH station, JUOH station is always considered as the virtual source to compare the same waveforms all along this study.

4.1.3 Ground motion prediction using the ambient seismic field

Amplitude of the impulse response functions needs to be calibrated with earthquake records. A low-magnitude earthquake that occurred close to the virtual source station can be used to compute the calibration factors λ_{ii} using eq. (3). Then, these values can be extrapolated to larger magnitude earthquakes that occurred in the same area just by using a simple scaling law. We use the scaling law developed by Aki (1967), which states that the Fourier spectra of two earthquakes

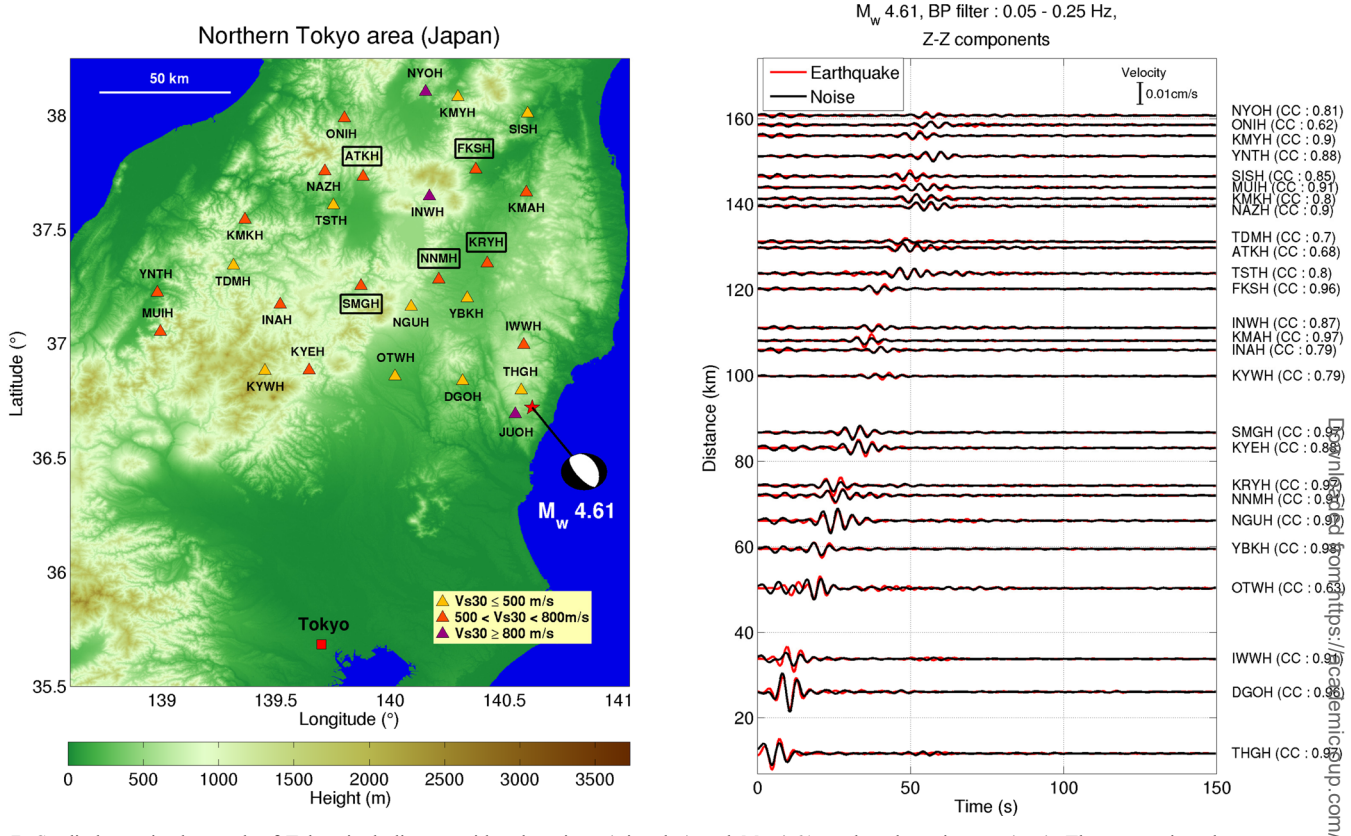

Figure 7. Studied area in the north of Tokyo including considered stations (triangles) and M_w 4.61 earthquake epicentre (star). The comparison between ambient noise impulse response waveforms (black lines) and earthquake records (red lines) bandpass filtered between 0.05 and 0.25 Hz in velocity for vertical components are shown in function of the distance to the virtual source (JUOH). Correlation coefficients *CC* are indicated between parentheses. The colour version of this figure is available only in the electronic edition.

differing by one surface wave magnitude order are separated by a factor of 10 at a period of 20 s in an ω-square model.

We use the records of an earthquake of magnitude M_w 4.01 located in the vicinity of the virtual source (see Table 1 for characteristics) together with the ambient noise impulse responses to compute the initial calibration factor λ_{ii}. Then, the scaling law is used to obtain an estimation of this factor (called λ_{pii} in the following) by which each component of the impulse responses has to be multiplied to predict the amplitude of earthquakes of magnitude M_w 5.02 and 5.82. Fig. 8 shows the difference between impulse responses multiplied by the predicted factor λ_{pii} (black lines) and the earthquake records (red lines). For each earthquake, impulse responses multiplied by the calibration factor λ_{ii} computed from the earthquake records and ambient noise impulse responses using eq. (3) are also shown (dashed lines). All these waveforms are shown for radial, transverse and vertical components in the frequency range of 0.05–0.25 Hz. The selected stations (station names framed in Fig. 1) have a V_{S30} greater than 500 m s^{-1} and are the ones used in the following to compute combined accelerograms. The phase of the waveforms computed with the ambient seismic field and the ones of the M_w 5.02 and 5.82 earthquakes are very similar to each other as indicated by high correlation coefficients. The amplitude of the impulse responses multiplied by the predicted factor λ_{pii} is lower than the impulse responses multiplied by the calibration factor λ_{ii} for these two events. Yet, a good phase and amplitude agreement between these three waveforms can be observed for the M_w 5.02 and 5.82 earthquakes indicating that the scaling law can be used to predict ground motions of $M_w \sim 6$ earthquakes. It can be noted that the correlation coefficient of the M_w 4.01 are the lowest. Indeed, the magnitude M_w 4.01 earthquake does not release enough energy at low frequencies and thus, signal is mainly dominated by the noise.

A comparison between the values of the computed (λ_{ii}) and predicted (λ_{pii}) normalization factors for different earthquakes from the magnitude M_w 4.01 event up to the M_w 5.82 earthquake (Table 1) is shown in Fig. 9. In spite of the fact that the theoretical scaling factor is effective at a period of 20 s, both amplitude factors are close to each other for each component up to the magnitude M_w 5.82 earthquake. Thus, the use of the scaling law to compute the calibration factor λ_{pii} could be useful to obtain a good estimation of the amplitude of moderate earthquakes (at least up $M_w \sim 6$) occurring in the same area. In the following, we use the factor λ_{ii} to scale the amplitude of the larger magnitude event before to compute the combined accelerograms.

4.2 Stochastic simulation results

As the impulse response functions are estimated between two stations, we computed the non-stationary simulations by taking into account the distance between the virtual source (JUOH) and the stations NNMH, KRYH, SMGH, FKSH and ATKH (station names framed in Fig. 1). These stations are located between 72 and 129.8 km from the virtual source and their V_{S30} values are between 507.6 and 596.0 m s^{-1}. Using the method developed by Laurendeau (2013), we computed 150 simulations for each station for a M_w 5.82 earthquake. Fig. 10 shows the geometric mean $\pm 1\sigma$ (light grey) and $\pm 2\sigma$ (dark grey) of 150 stochastic simulation Fourier spectra for radial and transverse components at NNMH station. In this figure, radial and transverse component accelerograms of the M_w 5.82 event recorded by the KiK-net network are also shown in black. As an anti-alias filter at 30 Hz is applied to the KiK-net

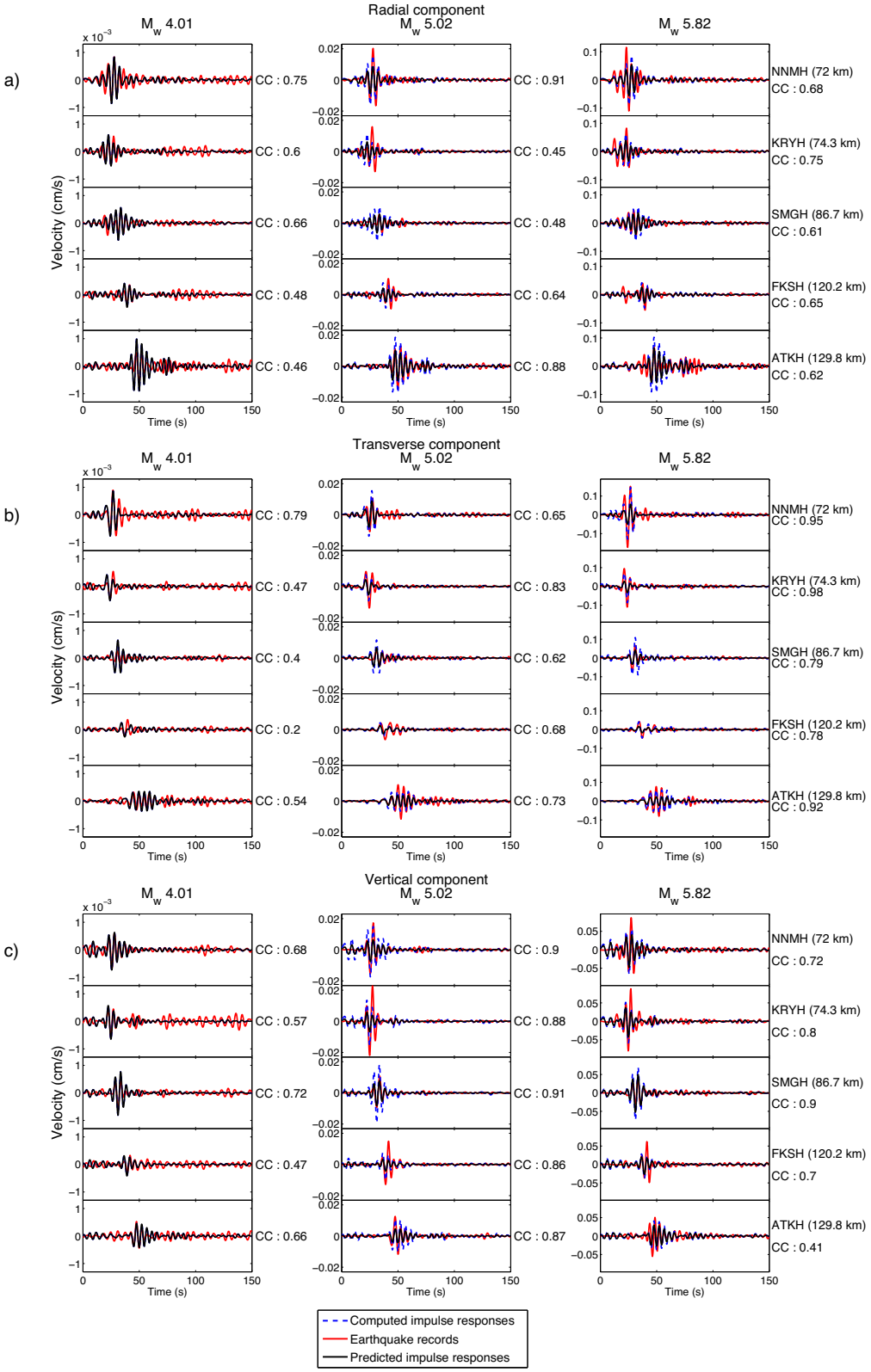

Figure 8. Prediction of M_w 5.02 and 5.82 earthquakes by multiplying the impulse responses with the normalization factors λ_{pRR} (a), λ_{pTT} (b) and λ_{pUU} (c) computed with an earthquake of magnitude 4.01 and extrapolated to higher magnitudes with the scaling law (black lines). Earthquakes are shown in red and impulse responses multiplied by normalization factors computed using each earthquake (λ_{RR}, λ_{TT} and λ_{UU}) are shown in dashed lines. The frequency range is between 0.05 and 0.25 Hz and distances indicated between parentheses are the distances between the virtual source (JUOH) and each station. The correlation coefficient CC are also shown. The colour version of this figure is available only in the electronic edition.

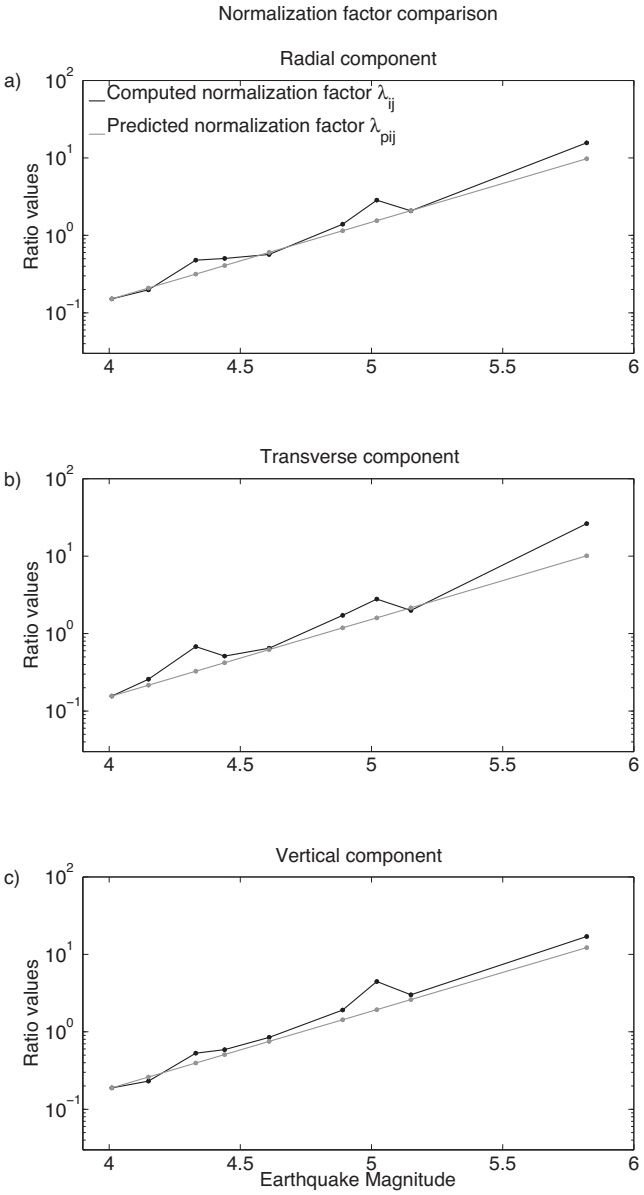

Figure 9. Comparison of the predicted factors (λ_{pii}) using an earthquake of magnitude M_w 4.01 and the scaling law to extrapolate to larger magnitude earthquake (grey) and the factors computed using each earthquake (λ_{ii}) in black computed from all the considered stations. These factors are shown for radial (a), transverse (b) and vertical (c) components.

records, Fourier spectra are only shown up to this frequency in the following.

In the frequency range of 0.05–30 Hz, the KiK-net records of both components are in the range of the simulations including the local site amplification between 7 and 20 Hz. However, as described by Laurendeau (2013), a point source model leads to an overestimated low-frequency content of the spectrum for high-magnitude earthquakes. This overestimation of the simulated accelerogram spectra can be observed at low frequencies (below 0.1 Hz) in Fig. 10 where the earthquake records are almost outside the range of the simulations. Even if the ambient noise impulse response gives also a point-source approximation, the recovered low-frequency content carries deterministic information from the source and the crust at long wavelengths. Thus, coupling the stochastic method with a

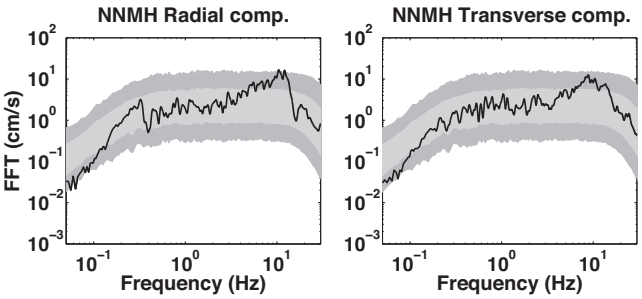

Figure 10. Comparison between radial and transverse components of KiK-net records Fourier spectra (black lines) and the geometric mean $\pm 1\sigma$ (light grey) and $\pm 2\sigma$ (dark grey) of 150 stochastic simulation Fourier spectra of an M_w 5.82 earthquake at NNMH station.

deterministic method can improve the results of broad-band simulations at low frequencies.

4.3 Combined results and discussion

Recall that Hi-net sensors are installed at depth. The method developed by Laurendeau (2013) predicts the ground motion at the surface using K-NET and KiK-net data. Combining the low-frequency part with the stochastic simulations supposes that the former has a wavelength large enough that the borehole depth is not seen. To confirm this hypothesis, KiK-net waveforms of the both events at the surface and at depth have been compared for these stations and present very close waveforms in the frequency range of 0.05–0.25 Hz.

The goal of this method is not to match the earthquake records but to provide traces having similar engineering characteristics of the target earthquake, namely Peak Ground Acceleration (PGA), energy, duration and non-stationarity. Fig. 11 shows the radial component in acceleration, velocity and displacement of KiK-net (black lines) and 9 of the 150 combined broad-band time histories (dark grey lines) for the earthquake of magnitude M_w 5.82 at NNMH station. Signals are bandpass filtered between 0.05 and 30 Hz. For this event, Peak Ground Displacements (PGDs) of the combined simulations presented here are included in the range of 0.26–0.46 cm. The PGD of the earthquake recorded at this station by the KiK-net network is 0.3 cm and is included in the range of the combined simulation PGDs. Peak Ground Velocity (PGV) and PGA of the observed earthquake are also in the range of the ones of the simulations. It may be also noted that the simulated PGVs are mainly higher than the one of the earthquake and that most of the PGAs are lower. Finally, simulated signals can generate strong ground motions with a duration longer than those of the recorded earthquake.

To compare the 150 synthesized ground motions to the M_w 5.82 event KiK-net records at every station, their accelerogram Fourier spectra were computed and plotted in Fig. 12. In this figure, radial and transverse components of the smooth KiK-net record spectra (black lines) are shown for NNMH (a), KRYH (b), SMGH (c), FKSH (d) and ATKH (e) stations. In bottom panels of each station, radial and transverse components of the combined simulations at the geometric mean $\pm 1\sigma$ level (light grey) and $\pm 2\sigma$ level (dark grey) are presented. To evaluate the improvements of our method, stochastic simulations computed with the method developed by Laurendeau (2013) are also shown in the top panels of each station in Fig. 12. In the frequency range of 0.1–0.25 Hz, the overestimation of the frequency content generated by stochastic simulations is removed in the combined simulations and amplitude spectra of

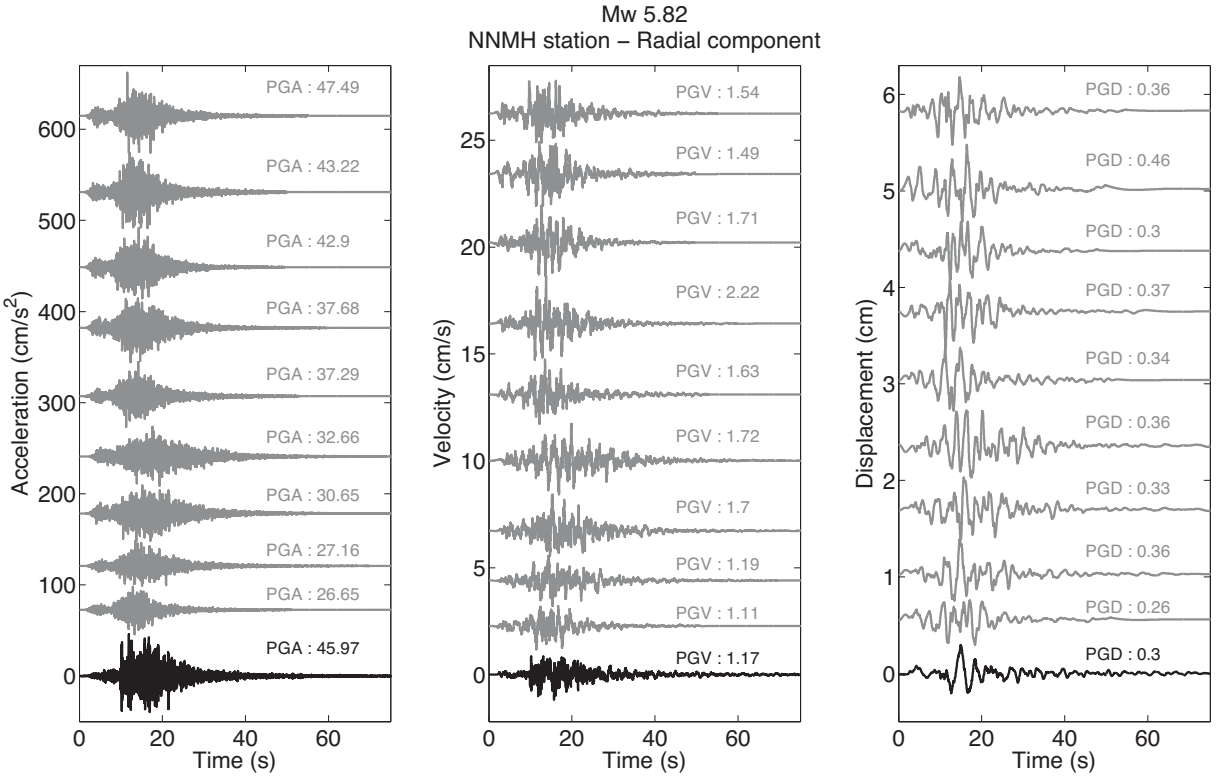

Figure 11. KiK-net radial component records (black lines) and combined simulations (dark grey lines) for the earthquake of magnitude M_w 5.82 recorded at NNMH station. From left to right, acceleration, velocity and displacement are shown. Peak Ground Acceleration (PGA), Peak Ground Velocity (PGV) and Peak Ground Displacement (PGD) values are also indicated.

KiK-net records are within or close to the range of the geometric mean $\pm 2\sigma$ for all the considered stations. One may note that the fit is however better for the transverse component than for the radial component for these stations. Indeed, a misfit can be observed at KRYH, ATKH and FKSH stations for the radial component below 0.1 Hz. Finally, broad-band simulation spectra have a shape similar to the earthquake record spectra but a slightly lower amplitude for stations. This feature can be explained by the fact that the virtual source–receiver distances are a few kilometres larger than the hypocentre–receiver distance, causing a larger geometrical decay. At high frequencies (>0.25 Hz), site effects inducing wave amplification at NNMH, KRYH and SMGH stations are within the range of the simulations.

Combining these two methods to estimate ground motion is an efficient way to generate broad-band acceleration time-series. The deterministic low-frequency part of the simulation allows us to take into account the information about the source and the path effects and thus, reduces the variability of the simulations in this frequency range. We showed that the simulated earthquake time-series are consistent with their observations ensuring the viability of this method.

5 CONCLUSIONS

In this study, we demonstrated that the ambient seismic field is a useful tool to investigate ground motions from future earthquakes. The frequency range available from noise data depends on the distance between the stations. Indeed, stations separated by distances less than 10 km synthesize ground motions up to 1 Hz. This frequency band decreases as the interstation distance increases. Yet, this technique could be a powerful tool to assess the seismic hazard for engineering purposes.

The amplitude of impulse responses always needs to be calibrated with earthquake records to predict ground motions. This might be a drawback of this technique in areas having a low-seismicity activity. Denolle *et al.* (2013) developed a technique to take into account the source depth and the focal mechanism effects. This might be further used to improve the ambient noise impulse response functions. Yet, the results obtained here are good enough because the attained frequency range already provides a relatively accurate prediction compared to observed data. Needless to say that regions where no velocity structure is known, this is a viable solution.

The stochastic method developed by Sabetta & Pugliese (1996), modified by Pousse *et al.* (2006) with improvements of Laurendeau (2013) also shows good results for the simulation of horizontal components. Combining both, the ambient noise impulse responses and the stochastic ground motion model, allows us to generate broad-band seismograms that agree quite well with the observations. The deterministic low-frequency part of the simulations contains the information on the physical structure of the upper crust and enables more precise ground motion predictions for frequencies of engineering interest. However, other techniques that simulate the high frequencies of ground motion could also be used (i.e. empirical Green's functions).

ACKNOWLEDGEMENTS

The authors thank the two anonymous reviewers who gave useful comments for improving the paper. We acknowledge the NIED of Japan for providing the K-NET, KiK-net and Hi-net continuous

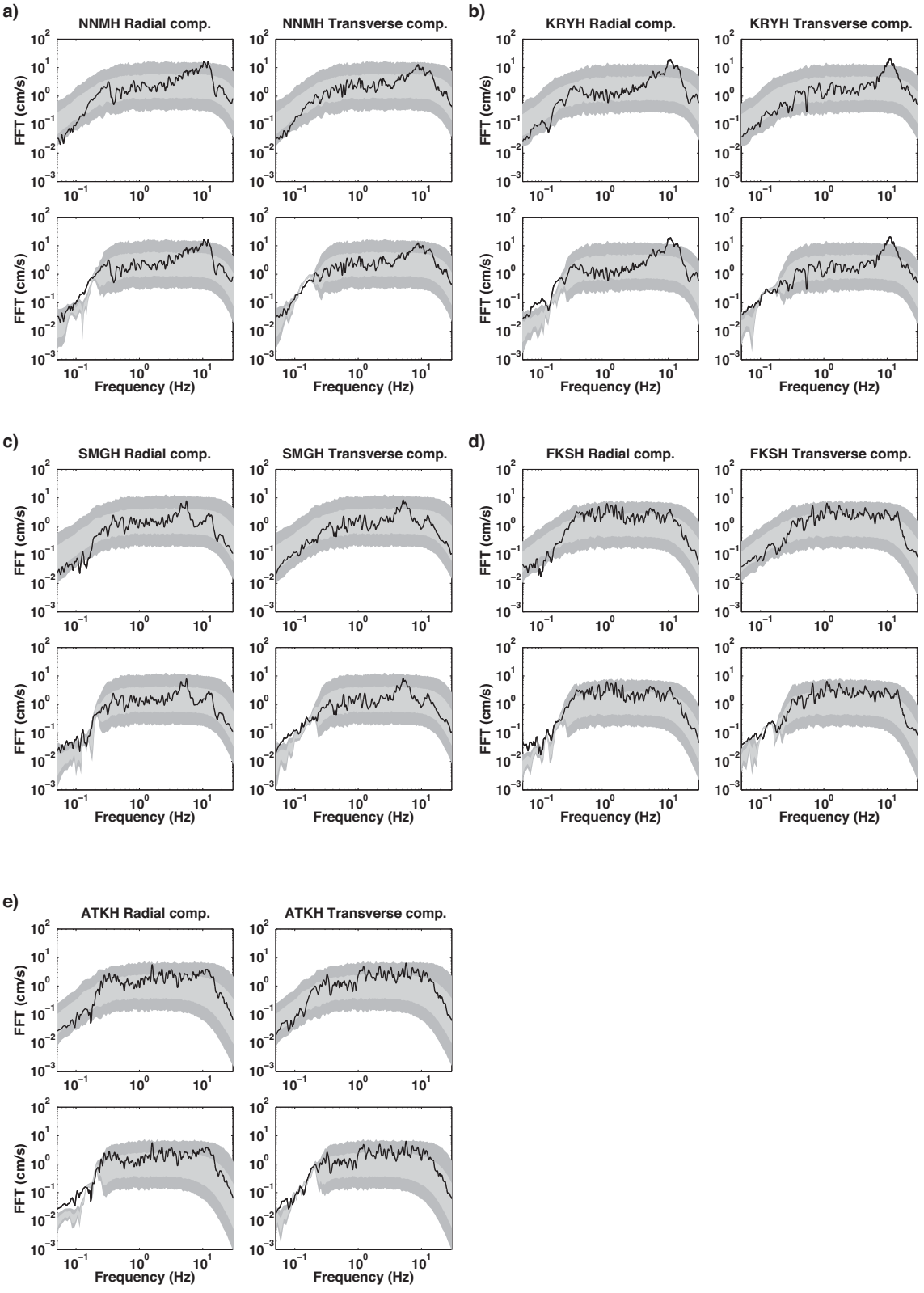

Figure 12. Accelerogram Fourier spectra of signals at NNMH (a), KRYH (b), SMGH (c), FKSH (d) and ATKH (e) stations. KiK-net accelerogram spectra of the M_w 5.82 earthquake records are shown in black. For each station, top panels show the radial and transverse components of the stochastic simulations at the geometric mean $\pm 1\sigma$ level (light grey) and $\pm 2\sigma$ level (dark grey). Bottom panels show the radial and transverse combined simulations at the geometric mean $\pm 1\sigma$ level (light grey) and $\pm 2\sigma$ level (dark grey).

data. We also thank the Japan Meteorological Agency (JMA) for the information about the earthquakes. We also thank Hiroe Miyake for valuable discussions on the ambient seismic field analysis. The work of NS was supported by an FP7 ERC Advanced grant 227507 (WHISPER).

REFERENCES

Abrahamson, N. & Youngs, R., 1992. A stable algorithm for regression analyses using the random effects model, *Bull. seism. Soc. Am.,* **82**(1), 505–510.

Aki, K., 1967. Scaling law of seismic spectrum, *J. geophys. Res.,* **72**(4), 1217–1231.

Aki, K. & Richards, P., 2002. *Quantitative Seismology, Geology: Seismology,* University Science Books.

Aoi, S., Kunugi, T. & Fujiwara, H., 2004. Strong-motion seismograph network operated by NIED K-NET and KiK-net, *J. Japan Assoc. Earthq. Eng.,* **4(3),** 65–74.

Arias, A., 1970. A measure of earthquake intensity, in *Seismic Design for Nuclear Power Plants,* pp. 438–483, ed. Hansen, R.J.. MIT Press. Cambridge, Massachusetts.

Bensen, G.D., Ritzwoller, M.H., Barmin, M.P., Levshin, A.L., Lin, F., Moschetti, M.P., Shapiro, N.M. & Yang, Y., 2007. Processing seismic ambient noise data to obtain reliable broad-band surface wave dispersion measurements, *Geophys. J. Int.,* **169**(3), 1239–1260.

Bommer, J., Stafford, P. & Alarcon, J., 2009. Empirical equations for the prediction of the significant, bracketed, and uniform duration of earthquake ground motion, *Bull. seism. Soc. Am.,* **99**(6), 3217–3233.

Bommer, J.J. & Acevedo, A.B., 2004. The use of real earthquake accelerograms as input to dynamic analysis, *J. Earthq. Eng.,* **8**(Suppl 001), 43–91.

Boore, D.M., 1983. Stochastic simulation of high-frequency ground motions based on seismological models of the radiated spectra, *Bull. seism. Soc. Am.,* **73**(6A), 1865–1894.

Boore, D.M., 2003. Simulation of ground motion using the stochastic method, *Pure appl. Geophys.,* **160**(3-4), 635–676.

Boore, D. & Atkinson, G., 2008. Ground-motion prediction equations for the average horizontal component of PGA, PGV, and 5%-damped PSA at spectral periods between 0.01 s and 10.0 s, *Earthq. Spectra,* **24**(1), 99–138.

Campillo, M. & Paul, A., 2003. Long-range correlations in the diffuse seismic coda, *Science,* **299**(5606), 547–549.

Campillo, M., Roux, P. & Shapiro, N.M., 2011. Seismic, ambient noise correlation, in *Encyclopedia of Solid Earth Geophysics, Encyclopedia of Earth Sciences Series,* pp. 1230–1236, ed. Gupta, H., Springer-Verlag.

Causse, M., Chaljub, E., Cotton, F., Cornou, C. & Bard, P.-Y., 2009. New approach for coupling k'2 and empirical Green's functions: application to the blind prediction of broad-band ground motion in the Grenoble basin, *Geophys. J. Int.,* **179**(3), 1627–1644.

Cotton, F., Pousse, G., Bonilla, F. & Scherbaum, F., 2008. On the discrepancy of recent European ground-motion observations and predictions from empirical models: analysis of KiK-net accelerometric data and point-sources stochastic simulations, *Bull. seism. Soc. Am.,* **98**(5), 2244–2261.

Denolle, M.A., Dunham, E.M., Prieto, G.A. & Beroza, G.C., 2013. Ground motion prediction of realistic earthquake sources using the ambient seismic field, *J. geophys. Res.: Sol. Earth,* **118**(5), 2102–2118.

Denolle, M.A., Dunham, E.M., Prieto, G.A. & Beroza, G.C., 2014. Strong ground motion prediction using virtual earthquakes, *Science,* **343**(6169), 399–403.

Douglas, J. & Aochi, H., 2008. A survey of techniques for predicting earthquake ground motions for engineering purposes, *Surv. Geophys.,* **29**(3), 187–220.

Foulser-Piggott, R. & Stafford, P., 2012. A predictive model for Arias intensity at multiple sites and consideration of spatial correlations, *Earthq. Eng. Struct. Dyn.,* **41**(3), 431–451.

Frankel, A., Mueller, C., Barnhard, T., Perkins, D., Leyendecker, E., Dickman, N., Hanson, S. & Hopper, M., 1996, National seismic hazard maps, June 1996, U.S. Department of the Interior, U.S. Geol. Surv.

Gasparini, D. & Vanmarcke, E., 1976. Simulated earthquake motions compatible with prescribed response spectra [SIMQKE], evaluation of seismic safety of buildings. Rep., Massachusetts Institute of Technology.

Gouédard, P. *et al.*, 2008. Cross-correlation of random fields: mathematical approach and applications, *Geophys. Prospect.,* **56**(3), 375–393.

Hanks, T., 1982. fmax, *Bull. seism. Soc. Am.,* **72**(6A), 1867–1879.

Hartzell, S.H., 1978. Earthquake aftershocks as Green's functions, *Geophys. Res. Lett.,* **5**(1), 1–4.

Husid, R., 1969. Analisis de terremotos: analisis general, *Revista del IDIEM,* **8**(1), 21–42.

Irikura, K., 1983. Semi-empirical estimation of strong ground motions during large earthquake, *Bull. Disaster Prevent. Res. Inst.,* **33,** 63–104.

Kamae, K., Irikura, K. & Pitarka, A., 1998. A technique for simulating strong ground motion using hybrid Green's function, *Bull. seism. Soc. Am.,* **88**(2), 357–367.

Komatitsch, D., Liu, Q., Tromp, J., Süss, P., Stidham, C. & Shaw, J.H., 2004. Simulations of ground motion in the Los Angeles Basin based upon the spectral-element method, *Bull. seism. Soc. Am.,* **94**(1), 187–206.

Lai, S., 1982. Statistical characterization of strong ground motions using power spectral density function, *Bull. seism. Soc. Am.,* **72**(1), 259–274.

Laurendeau, A., 2013. Définitions des mouvements sismiques au rocher, *PhD thesis,* Université Joseph Fourier, Grenoble, France.

Lobkis, O.I. & Weaver, R.L., 2001. On the emergence of the Green's function in the correlations of a diffuse field, *J. acoust. Soc. Am.,* **110**(6), 3011–3017.

Obara, K., Kasahara, K., Hori, S. & Okada, Y., 2005. A densely distributed high-sensitivity seismograph network in Japan: Hi-net by National Research Institute for Earth Science and Disaster Prevention, *Rev. Sci. Instrum.,* **76**(2), 021301–021301–12.

Okada, Y., Kasahara, K., Hori, S., Obara, K., Sekiguchi, S., Fujiwara, H. & Yamamoto, A., 2004. Recent progress of seismic observation networks in Japan: Hi-net, F-net, K-NET and KiK-net, *Earth Planets Space,* **56,** xv–xxviii.

Olsen, K.B. *et al.*, 2006. Strong shaking in Los Angeles expected from southern San Andreas earthquake, *Geophys. Res. Lett.,* **33,** L07305, doi:10.1029/2005GL025472.

Peterson, J., 1993. Observations and modeling of seismic background noise, Open-File Rep, U.S. Geol. Surv., 93–322.

Pousse, G., Bonilla, L.F., Cotton, F. & Margerin, L., 2006. Nonstationary stochastic simulation of strong ground motion time histories including natural variability: application to the K-Net Japanese database, *Bull. seism. Soc. Am.,* **96**(6), 2103–2117.

Prieto, G.A. & Beroza, G.C., 2008. Earthquake ground motion prediction using the ambient seismic field, *Geophys. Res. Lett.,* **35**(14), L14304, doi:10.1029/2008GL034428.

Prieto, G.A., Parker, R.L. & Vernon, F.L. III2009. A Fortran 90 library for multitaper spectrum analysis, *Comput. Geosci.,* **35**(8), 1701–1710.

Pulido, N. & Kubo, T., 2004. Near-fault strong motion complexity of the 2000 Tottori earthquake (Japan) from a broadband source asperity model, *Tectonophysics,* **390**(1–4), 177–192.

Roux, P., Sabra, K.G., Gerstoft, P., Kuperman, W.A. & Fehler, M.C., 2005a. P-waves from cross-correlation of seismic noise, *Geophys. Res. Lett.,* **32,** L19303, doi:10.1029/2005GL023803.

Roux, P., Sabra, K.G., Kuperman, W.A. & Roux, A., 2005b. Ambient noise cross correlation in free space: Theoretical approach, *J. acoust. Soc. Am.,* **117**(1), 79–84.

Sabetta, F. & Pugliese, A., 1996. Estimation of response spectra and simulation of nonstationary earthquake ground motions, *Bull. seism. Soc. Am.,* **86**(2), 337–352.

Shapiro, N.M. & Campillo, M., 2004. Emergence of broadband Rayleigh waves from correlations of the ambient seismic noise, *Geophys. Res. Lett.,* **31,** L07614, doi:10.1029/2004GL019491.

Shapiro, N.M., Campillo, M., Stehly, L. & Ritzwoller, M.H., 2005. High-resolution surface-wave tomography from ambient seismic noise, *Science,* **307**(5715), 1615–1618.

Snieder, R., 2004. Extracting the Green's function from the correlation of coda waves: a derivation based on stationary phase, *Phys. Rev. E,* **69**(4), 046610, doi:10.1103/PhysRevE.69.046610.

Stockwell, R.G., Mansinha, L. & Lowe, R.P., 1996. Localization of the complex spectrum: the S transform, *IEEE Trans. Signal Process.,* **44**(4), 998–1001.

Thomson, D., 1982. Spectrum estimation and harmonic analysis, *Proc. IEEE,* **70**(9), 1055–1096.

Vasconcelos, I. & Snieder, R., 2008. Interferometry by deconvolution: part 1: theory for acoustic waves and numerical examples, *Geophysics,* **73**(3), S115–S128.

Wapenaar, K., 2004. Retrieving the elastodynamic Green's function of an arbitrary inhomogeneous medium by cross correlation, *Phys. Rev. Lett.,* **93,** 254301-1–254301-4.

Weaver, R.L. & Lobkis, O.I., 2001. Ultrasonics without a source: thermal fluctuation correlations at MHz frequencies, *Phys. Rev. Lett.,* **87,** 134301-1–134301-4.